

Burying non-radiative defects in InGaN underlayer to increase InGaN/GaN quantum well efficiency

C. Haller, J.-F. Carlin, G. Jacopin, D. Martin, R. Butté, and N. Grandjean

Citation: *Appl. Phys. Lett.* **111**, 262101 (2017);

View online: <https://doi.org/10.1063/1.5007616>

View Table of Contents: <http://aip.scitation.org/toc/apl/111/26>

Published by the [American Institute of Physics](#)

Articles you may be interested in

[Temperature-dependent transport properties of graphene decorated by alkali metal adatoms \(Li, K\)](#)
Applied Physics Letters **111**, 263502 (2017); 10.1063/1.5001080

[234 nm and 246 nm AlN-Delta-GaN quantum well deep ultraviolet light-emitting diodes](#)
Applied Physics Letters **112**, 011101 (2018); 10.1063/1.5007835

[BInGaN alloys nearly lattice-matched to GaN for high-power high-efficiency visible LEDs](#)
Applied Physics Letters **111**, 211107 (2017); 10.1063/1.4997601

[Spin-phonon coupling in antiferromagnetic nickel oxide](#)
Applied Physics Letters **111**, 252402 (2017); 10.1063/1.5009598

[Impact of carrier localization on recombination in InGaN quantum wells and the efficiency of nitride light-emitting diodes: Insights from theory and numerical simulations](#)
Applied Physics Letters **111**, 113501 (2017); 10.1063/1.5002104

[Field-assisted Shockley-Read-Hall recombinations in III-nitride quantum wells](#)
Applied Physics Letters **111**, 233501 (2017); 10.1063/1.5003112

Scilight

Sharp, quick summaries **illuminating**
the latest physics research

Sign up for **FREE!**

AIP
Publishing

Burying non-radiative defects in InGaN underlayer to increase InGaN/GaN quantum well efficiency

C. Haller, J.-F. Carlin, G. Jacopin, D. Martin, R. Butté, and N. Grandjean

Institute of Physics, Ecole polytechnique fédérale de Lausanne (EPFL), CH-1015 Lausanne, Switzerland

(Received 2 October 2017; accepted 7 November 2017; published online 26 December 2017)

The insertion of an InGaN underlayer (UL) is known to strongly improve the performance of InGaN/GaN quantum well (QW) based blue light emitting diodes (LEDs). However, the actual physical mechanism responsible for it is still unclear. We thus conduct a systematic study and investigate different hypotheses. To this aim, InGaN/GaN single (S) QWs are grown on sapphire and GaN free-standing substrates with or without InGaN UL. This allows us to conclude that (i) improvement of LED performance is due to a higher internal quantum efficiency of the InGaN/GaN SQW and (ii) reduction of structural defects is not at play. Furthermore, we show that neither the surface morphology nor the strain of the top GaN layer before the growth of the QW is affected by the InGaN UL. Finally, we find that the beneficial effect of the InGaN UL is still present after 100 nm of GaN. This result combined with band structure modelling rules out the hypothesis of higher QW oscillator strength induced by a reduction of the internal electric field due to band bending. In conclusion, we demonstrate that the increase in InGaN/GaN QW efficiency is the consequence of a reduction of non-radiative recombination centers in the QW itself, independent of the dislocation density. © 2017 Author(s). All article content, except where otherwise noted, is licensed under a Creative Commons Attribution (CC BY) license (<http://creativecommons.org/licenses/by/4.0/>). <https://doi.org/10.1063/1.5007616>

III-nitride blue-violet light-emitting diodes (LEDs) are nowadays widely commercialized for solid state lighting and can reach an internal quantum efficiency (IQE) higher than 80%.¹ To improve the performance of LEDs, epi-structures often include an InGaN underlayer (UL) before the growth of InGaN/GaN quantum wells (QWs) which constitute the active region. This InGaN UL, which is a few tens of nanometers thick, has a lower indium content than the active QWs to avoid absorption losses. The use of such a layer is well documented in the literature, and several mechanisms have been proposed to explain the subsequent improvement of LED efficiency.^{2–11} One of the hypotheses is that the InGaN UL favors the injection of free carriers by creating an electron reservoir, which allows for a better carrier capture efficiency by the QWs.^{2–6} However, the improvement of the photoluminescence (PL) properties of InGaN/GaN QWs suggests that the InGaN UL acts on the QW radiative efficiency itself. For instance, Törmä *et al.* proposed that such InGaN UL decreases the density of threading dislocations that affect the QW region.⁷ Another suggested mechanism involves the formation of pits at the dislocation surface termination.¹² These topographical V-defects may induce a screening of the threading dislocations for carriers thanks to a potential barrier located in their vicinity.¹³ Besides an improved structural quality, the InGaN UL has been proposed to affect the band profile due to pinning of the Fermi level at the InGaN/GaN interface, which in turn reduces the built-in electric field in the QWs and thus leads to an increase in the QW radiative efficiency.⁸ Likewise, Nanhui *et al.* proposed that the InGaN UL acts as a strain relief layer, lowering the internal piezoelectric-field and thus alleviating the detrimental impact of the quantum confined Stark effect (QCSE).⁹ Other studies have shown that the InGaN UL strongly reduces the

density of non-radiative recombination centers (NRCs) and that this decrease is mediated by In atoms.¹¹ Recently, Armstrong *et al.* confirmed by performing deep level optical spectroscopy that the improvement of LEDs is due to a reduction in the deep level density in the QW active region.¹⁰ At this stage, one should point out that these two studies do not allow ruling out dislocation reduction.⁷ Indeed, point defects can be found in the dislocation surrounding.¹⁴ Also, strain relief remains a strong candidate owing to the dependence of the point defect density with compressive strain in the InGaN alloy.¹⁵

In this paper, we carefully investigate the various aforementioned hypotheses and unambiguously demonstrate that the InGaN UL dramatically increases the IQE of InGaN QWs by reducing the point defect density independent of the dislocation density, the GaN surface morphology, or the strain state of the QWs.

The samples investigated in this work are grown in an Aixtron 3 × 2" CCS metalorganic vapor phase epitaxy (MOVPE) reactor. The substrates are either *c*-plane GaN/sapphire templates or *c*-plane free-standing (FS) GaN wafers with a dislocation density of a few 10⁸ cm⁻² or ~10⁶ cm⁻², respectively. The different sample structures (A to D) investigated in this work are displayed in Fig. 1. The GaN buffer is grown at 1000 °C with trimethylgallium (TMGa) and H₂ as carrier gas for all the samples. For structures C and D, the Al_{0.06}Ga_{0.94}N layer is deposited at 1000 °C with trimethylaluminum and TMGa with H₂ as carrier gas. For the growth of InGaN alloys, the carrier gas is switched to N₂. The 55 nm-thick In_{0.03}Ga_{0.97}N UL is grown at 770 °C with trimethylindium and triethylgallium (TEGa). The GaN spacer growth is performed with TEGa and at the same temperature as the InGaN UL. For these structures, the temperature is

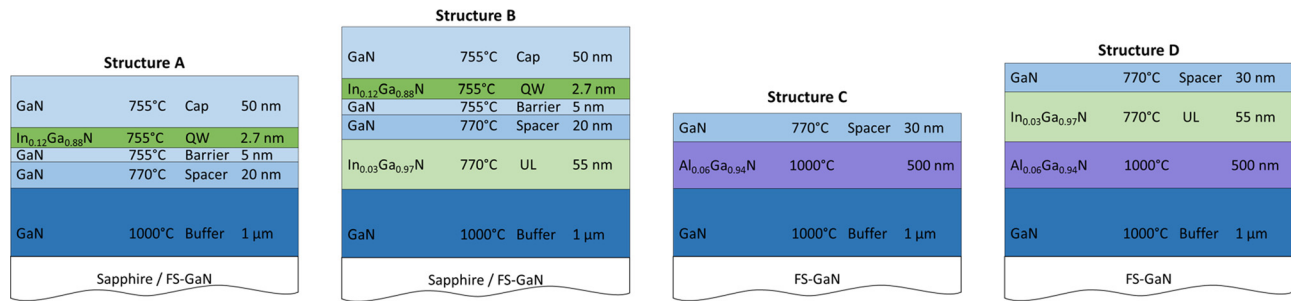


FIG. 1. Sketch of the different sample structures used in the present study.

reduced to 755 °C for the growth of the bottom barriers and the $\text{In}_{0.12}\text{Ga}_{0.88}\text{N}$ single (S) QW. The barrier and SQW thicknesses are 5 nm and 2.7 nm, respectively. Finally, a 50 nm thick cap layer is grown on top of the SQW at 755 °C.

SQW-LED structures with and without an InGaN UL were also fabricated on planar *c*-plane sapphire substrate using the same growth conditions as the samples based on structures A and B. The LED layer sequence consists of a 2 μm -thick Si-doped GaN layer ($n = 5 \times 10^{18} \text{ cm}^{-3}$), a 2.7 nm-thick $\text{In}_{0.12}\text{Ga}_{0.88}\text{N}$ SQW, a 20 nm-thick $\text{Al}_{0.2}\text{Ga}_{0.8}\text{N}$ electron blocking layer, and 100 nm of *p*-type GaN ($[\text{Mg}] = 1\text{--}2 \times 10^{19} \text{ cm}^{-3}$). In one of the LED structures, a 55 nm-thick $\text{In}_{0.03}\text{Ga}_{0.97}\text{N}$ UL is inserted between the Si-doped GaN and the SQW. The GaN spacer thickness between the SQW and the InGaN UL is equal to 20 nm. $300 \times 300 \mu\text{m}^2$ LEDs were processed with Ti/Al/Ti/Au and Pd/Au metal stacked layers for *n*- and *p*-type contacts, respectively. The emission wavelength is 415 nm, and the electroluminescence (EL) intensity is measured from the backside of the device with a calibrated photodiode. Such measurements performed on SQW-LEDs featuring an InGaN UL lead to a maximum external quantum efficiency (EQE) value of about 8%. This value is much lower than the state of the art EQE values, but one shall consider that (i) the extraction efficiency is low for LEDs grown on planar sapphire substrate, (ii) light is collected only from the backside of the device, and (iii) the active region consists of a SQW and the injection efficiency is not optimized.

First, we compared the performance of SQW-LEDs with and without InGaN UL [Fig. 2(a)]. As expected, the maximum EQE of LEDs with an InGaN UL is dramatically improved ($\times 3.5$) with respect to that of LEDs without that

layer. The current density at which the normalized EQE is maximum is 50 times higher for the latter. To be more quantitative, we apply the ABC model accounting for radiative and non-radiative recombination channels to the data [dotted line in Fig. 2(a)].¹⁶ As the QW structure is the same, we fix B and C coefficients which account for radiative recombination ($B = 8.6 \times 10^{-11} \text{ cm}^3 \text{ s}^{-1}$) and Auger recombination ($C = 1.6 \times 10^{-29} \text{ cm}^6 \text{ s}^{-1}$), respectively. Only the A coefficient (Shockley-Read-Hall coefficient) is allowed to change between the two fits. This leads to a reduction of the A coefficient by almost two orders of magnitude when an InGaN UL is introduced in the LED structure. However, at this stage, one cannot discriminate between a better electrical injection efficiency, favored by the InGaN UL,²⁻⁶ and a higher IQE of the $\text{In}_{0.12}\text{Ga}_{0.88}\text{N}$ SQW.⁷⁻¹² In order to assess the properties of the active region itself, we prepared SQW samples on GaN/sapphire templates without (structure A) and with (structure B) an InGaN UL. Then, we performed quasi-resonant PL measurements at room-temperature using a 375 nm continuous wave laser diode. Notice that the combination of low power density (5.9 W/cm^2) and sub-bandgap GaN excitation (absorption occurring in the QW only) guarantees a small photogenerated carrier density, which makes such PL experiments very sensitive to NRCs.

Figure 2(b) shows the PL spectra of InGaN SQW samples grown on GaN/sapphire templates with and without InGaN UL. The QW emission intensity is nearly two orders of magnitude higher with the InGaN UL. Since the carriers are photo-generated only in the QW, one may conclude that the effect of the InGaN UL is to increase the QW efficiency. However, the PL intensity also depends on the surface roughness, e.g., a rough surface could increase the light

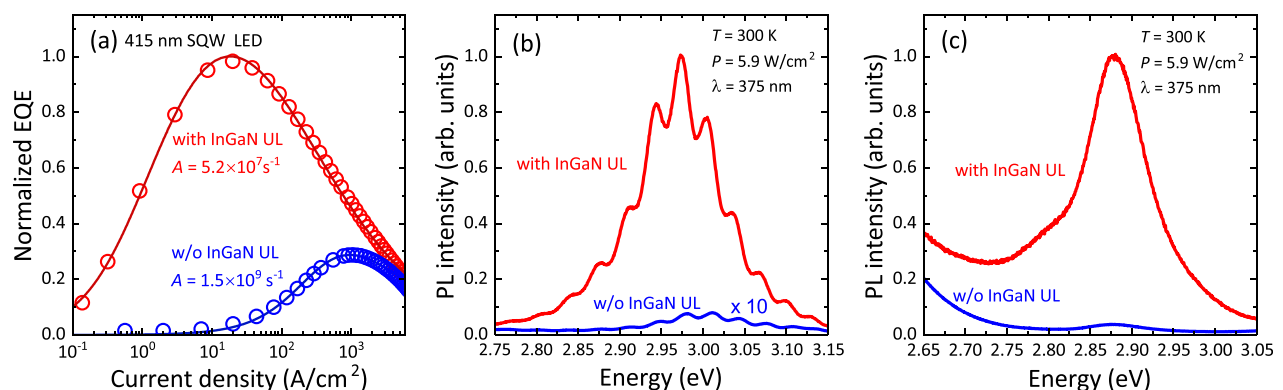


FIG. 2. Relative EQE versus current density of SQW LEDs normalized to the most efficient one (a) and 300 K PL intensity of an $\text{In}_{0.12}\text{Ga}_{0.88}\text{N}/\text{GaN}$ SQW grown on GaN/sapphire template (b) and on FS GaN substrate (c), with (red lines) and without (blue lines) an InGaN UL.

extraction. We thus carried out atomic force microscopy (AFM) measurements to get access to the morphology of the top surface. It can be seen in Figs. 3(a) and 3(b) that the surfaces are not markedly different. The root mean square (rms) surface roughness values are 3.9 nm and 2.6 nm for a surface of $5 \times 5 \mu\text{m}^2$, with and without the UL, respectively. These values are sufficiently close to each other to confirm that the stronger PL signal is due to the higher radiative efficiency of the QW grown with an InGaN UL. The latter could thus reduce the dislocation density⁷ and/or modify the surface morphology before the growth of the QW starts. To look at this, we additionally grew samples with structures A and B, but without the QW and cap layers, on 1/6th of the same GaN/sapphire template to ensure similar initial material quality. AFM images of these samples are shown in Figs. 3(c) and 3(d). A statistical analysis performed on several scans shows that the pit density is about $2 \times 10^8 \text{ cm}^{-2}$ and $6 \times 10^8 \text{ cm}^{-2}$ for samples without and with an InGaN UL, respectively. Whereas the pit density does not exactly correspond to the dislocation density, it provides some qualitative information about the structural properties. The slightly higher pit density found for the sample with an InGaN UL leaves us with two partial conclusions: (i) we cannot

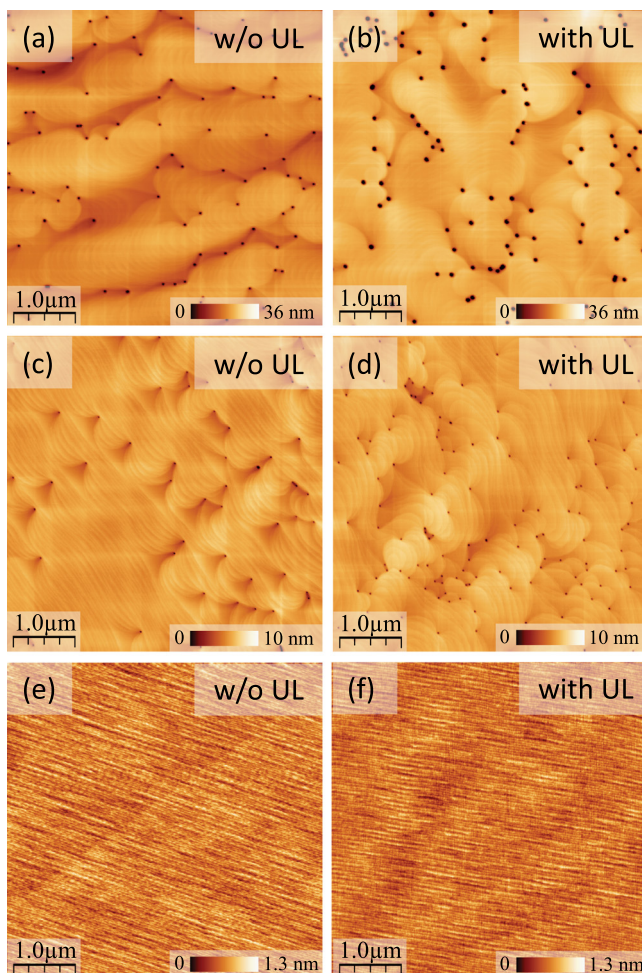


FIG. 3. $5 \times 5 \mu\text{m}^2$ AFM images: $\text{In}_{0.12}\text{Ga}_{0.88}\text{N}/\text{GaN}$ SQW grown on GaN/sapphire template without (a) and with (b) an InGaN UL. GaN spacer on GaN/sapphire template without (c) and with an InGaN UL (d). GaN spacer on FS GaN substrate without (e) and with an InGaN UL (f).

conclude that the InGaN UL reduces the dislocation density and (ii) the InGaN UL promotes the pit formation because of the lower surface energy of the InGaN alloy.¹⁷ At first sight, our results seem to be consistent with the dislocation-screening mechanism induced by the formation of V-defects at the dislocation surface termination,¹³ as proposed in a couple of papers.^{12,18}

To clarify this point, we moved to FS GaN substrates for which the dislocation density ($\sim 10^6 \text{ cm}^{-2}$) is at least two orders of magnitude lower than that on sapphire. We first looked at the impact of the UL on the surface morphology before the growth of the QW starts. To this aim, two samples with structures A and B but without the QW and the cap layer have been grown on FS GaN. The surface morphology of the GaN spacer, as seen by AFM, is displayed in Figs. 3(e) and 3(f). First, the regularity of the terraces over a $5 \times 5 \mu\text{m}^2$ scan ascertains the low dislocation density of the GaN substrate. Second, the surface morphology of the GaN spacer seems to not be affected by the InGaN UL, i.e., the InGaN SQW is deposited on the same surface morphology.

We investigated the PL properties of an $\text{In}_{0.12}\text{Ga}_{0.88}\text{N}$ SQW grown on the FS GaN substrate without and with an InGaN UL (structures A and B). The corresponding 300 K PL spectra obtained with non-resonant laser excitation are displayed in Fig. 2(c). A huge difference in the PL intensity is still observed. One can thus conclude that the increase in the QW efficiency induced by the InGaN UL is neither related to a reduction in the dislocation density nor to a screening of the dislocations by V-defects.

One of the particularities of the InGaN/GaN QWs grown along the *c*-axis is the existence of a built-in field, which is mostly of piezoelectric origin. This electric field pulls apart the electron and hole wave functions and decreases the oscillator strength, especially for thick wells. This is the so-called QCSE. It was proposed that the increase in the QW radiative efficiency arises from a reduction of the internal electric field due to band bending induced by the pinning of the Fermi level at the InGaN/GaN interface.⁸ We computed the band structure of a 2.7 nm thick $\text{In}_{0.12}\text{Ga}_{0.88}\text{N}$ SQW with and without an InGaN UL and for various spacer thicknesses (the distance between the QW and the InGaN UL) and different doping levels.¹⁹ The evolution of the QW oscillator strength is reported in Fig. 4(a). Our simulations indeed confirm an increase in the oscillator strength for spacer thicknesses less than 20 nm. This is in agreement with Ref. 8 in which the spacer is only 3 nm thick. However, our results show a maximum gain of 60%, which reduces to 30% when considering our actual structure parameters. Note that the limited impact of the electric field on the oscillator strength is due to the rather thin QW thickness we use. Consequently, our simulations cannot account for the observed huge experimental IQE increase. Furthermore, for spacers thicker than 20 nm, the model indicates that the InGaN UL should no longer influence the oscillator strength. To challenge the simulation data, we grew on FS GaN substrates 3 samples with structure B but with different spacer thicknesses (20, 50, and 100 nm). Figure 4(b) displays the PL intensity, measured at 300 K under non-resonant laser excitation, of this sample series. The PL intensity is constant whatever the spacer thickness and is one order of magnitude higher than the PL intensity of

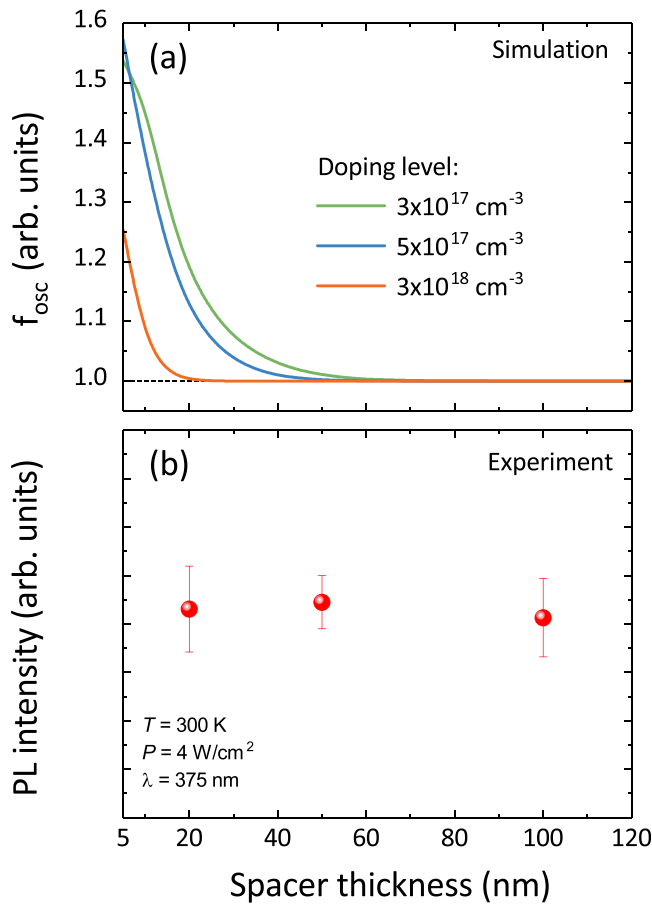


FIG. 4. Oscillator strength calculated for a 2.7 nm thick $\text{In}_{0.12}\text{Ga}_{0.88}\text{N}/\text{GaN}$ SQW as a function of spacer thickness and for different doping levels (a) and PL intensity of $\text{In}_{0.12}\text{Ga}_{0.88}\text{N}/\text{GaN}$ SQWs grown on FS GaN substrates with an InGaN UL and for spacer thicknesses of 20, 50, and 100 nm (b).

the SQW without InGaN UL. This demonstrates that the beneficial impact of the InGaN UL is still effective after 100 nm of GaN.

One of the last hypotheses is that the InGaN UL influences the strain state and thereby reduces the piezoelectric field⁹ and/or the point defect density.¹⁵ With the aim of probing the strain which could be induced by the InGaN UL, we designed specific structures (C and D) where we can probe the band edge of a very thin GaN layer (30 nm) and deduce thereby the strain from well-identified low temperature transition energies like the A free-exciton or the neutral donor bound exciton.²⁰ To optically isolate this layer from the GaN buffer luminescence, we introduced a 500 nm thick $\text{Al}_{0.06}\text{Ga}_{0.94}\text{N}$ buffer layer, which is aimed at absorbing most of the excitation laser power. PL experiments were performed with a 325 nm HeCd laser at 11 K with a pump power density of 0.4 W/cm^2 . Figure 5 displays the band edge spectra of the 30 nm thick GaN layer without (blue) and with (red) an InGaN UL. The free A exciton (FX_A) and the free B exciton (FX_B) are more pronounced in the case of the sample without the InGaN UL. This can be understood by exciton diffusion toward the InGaN UL where they eventually recombine. On the other hand, the neutral donor bound A excitons (D^0X_A), being localized, are clearly visible in both samples. The transition energies of D^0X_A and FX_A are 3.473 eV and 3.480 eV, respectively, for both samples. These transition energies are close to those reported for unstrained GaN.²¹ We

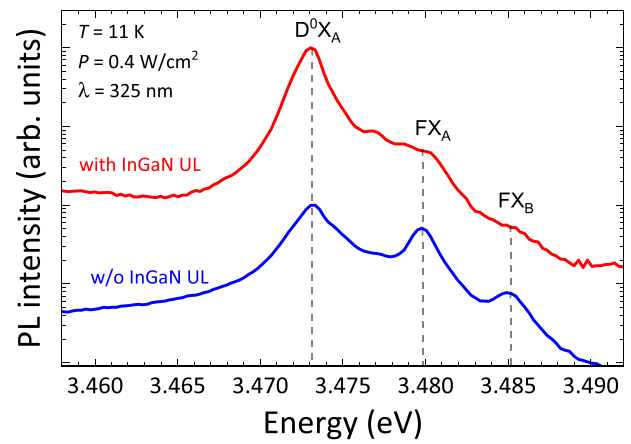


FIG. 5. PL spectra, shifted for clarity, of a 30 nm thick GaN spacer with (red lines) and without (blue lines) an InGaN UL.

performed PL experiments at several locations and observed a small energy variation ($\sim 0.3 \text{ meV}$). This corresponds to stress fluctuations of about 0.4 kbar, which might be related to strain inhomogeneities in the FS GaN substrate. From this low-temperature GaN band edge luminescence spectroscopy, we conclude that the strain state of the GaN layer is identical for the two samples.

In conclusion, after discriminating between various mechanisms, the most likely role of the InGaN UL used in LEDs is the reduction of defects and/or impurities, as proposed by Armstrong *et al.*¹⁰ This is in line with the reduction of the A coefficient observed for SQW LEDs featuring an InGaN UL. However, the nature of these defects is not clear yet. Secondary ion mass spectroscopy (SIMS) was performed on the studied samples to look for O, C, Mg, Fe, and Ca. SIMS measurements did not reveal any striking differences regarding the concentration level of those impurities. This could be due to the SIMS detection limit or other impurities we missed. Nevertheless, we hypothesize that a detrimental species is present at the GaN surface. This species reacts with indium atoms forming non-radiative complexes in the InGaN alloy. The role of the InGaN UL is thus to bury such species before the growth of the active InGaN QWs and to avoid the formation of these non-radiative complexes in the well itself.

The authors would like to thank Dr. K. Shojiki and Dr. G. Callsen for useful discussion and Dr. M. Mosca and M. Lupatini for the LED processing and EL measurements. This work was supported by the CTI-KTI Project ‘‘High power GaN-lasers for white light generation’’ 17519.1 PFEN-NM. G.J. acknowledges financial support from the SNSF under project No. 154853.

¹A. David, N. G. Young, C. A. Humi, and M. D. Craven, *Appl. Phys. Lett.* **110**, 253504 (2017).

²Y. Xia, W. Hou, L. Zhao, M. Zhu, T. Detchprohm, and C. Wetzel, *IEEE Trans. Electron Devices* **57**, 2639 (2010).

³Y. Takahashi, A. Satake, K. Fujiwara, J. K. Shue, U. Jahn, H. Kostial, and H. T. Grahn, *Physica E* **21**, 876 (2004).

⁴J.-Y. Park, J.-H. Lee, S. Jung, and T. Ji, *Phys. Status Solidi A* **213**, 1610 (2016).

⁵N. Otsuji, K. Fujiwara, and J. K. Sheu, *J. Appl. Phys.* **100**, 113105 (2006).

⁶J.-W. Ju, E.-S. Kang, H.-S. Kim, L.-W. Jang, H.-K. Ahn, J.-W. Jeon, I.-H. Leea, and J. H. Baek, *J. Appl. Phys.* **102**, 053519 (2007).

- ⁷P. T. Törmä, O. Svensk, M. Ali, S. Suihkonen, M. Sopanen, M. A. Odnoblyudov, and V. E. Bougrov, *J. Cryst. Growth* **310**, 5162 (2008).
- ⁸M. J. Davies, P. Dawson, F. C.-P. Massabuau, A. L. Fol, R. A. Oliver, M. J. Kappers, and C. J. Humphreys, *Phys. Status Solidi B* **252**, 866 (2015).
- ⁹N. Nanhui, W. Huaibing, L. Jianping, L. Naixin, X. Yanhui, H. Jun, D. Jun, and S. Guangdi, *J. Cryst. Growth* **286**, 209 (2006).
- ¹⁰A. M. Armstrong, B. N. Bryant, M. H. Crawford, D. D. Koleske, S. R. Lee, and J. J. Wierer, *J. Appl. Phys.* **117**, 134501 (2015).
- ¹¹T. Akasaka, H. Gotoh, T. Saito, and T. Makimoto, *Appl. Phys. Lett.* **85**, 3089 (2004).
- ¹²Y. Chen, T. Takeuchi, H. Amano, I. Akasaki, N. Yamada, Y. Kaneko, and S. Y. Wang, *Appl. Phys. Lett.* **72**, 710 (1998).
- ¹³A. Hangleiter, F. Hitzel, C. Netzel, D. Fuhrmann, U. Rossow, G. Ade, and P. Hinze, *Phys. Rev. Lett.* **95**, 127402 (2005).
- ¹⁴A. Hierro, M. Hansen, L. Zhao, J. S. Speck, U. K. Mishra, S. P. DenBaars, and S. A. Ringel, *Phys. Status Solidi B* **228**, 937 (2001).
- ¹⁵T. Langer, A. Chernikov, D. Kalincev, M. Gerhard, H. Bremers, U. Rossow, M. Koch, and A. Hangleiter, *Appl. Phys. Lett.* **103**, 202106 (2013).
- ¹⁶L. A. Coldren, S. W. Corzine, and M. Mashanovitch, *Diode Lasers and Photonic Integrated Circuits*, 2nd ed. (Wiley, Hoboken, NJ, 2012).
- ¹⁷N. Sharma, P. Thomas, D. Tricker, and C. Humphreys, *Appl. Phys. Lett.* **77**, 1274 (2000).
- ¹⁸H. Takahashi, A. Ito, T. Tanaka, A. Watanabe, H. Ota, and K. Chikuma, *Jpn. J. Appl. Phys., Part 2* **39**, L569 (2000).
- ¹⁹S. Birner, *Nextnano++ simulation software* (Nextnano GmbH).
- ²⁰B. Gil, O. Briot, and R.-L. Aulombard, *Phys. Rev. B* **52**, R17028 (1995).
- ²¹K. Kornitzer, T. Ebner, K. Thonke, R. Sauer, C. Kirchner, V. Schwegler, M. Kamp, M. Leszczynski, I. Grzegory, and S. Porowski, *Phys. Rev. B* **60**, 1471 (1999).